

# Energy-Aware Ergodic Search: Continuous Exploration for Multi-Agent Systems with Battery Constraints

Adam Seewald, Cameron J. Lerch, Marvin Chancán, Aaron M. Dollar, and Ian Abraham

**Abstract**—Exploring space without interruption is important in scenarios such as search and rescue and precision agriculture. Ergodic search already derives continuous trajectories in these scenarios so that the robots spend more time in areas with high information density. However, existing literature on ergodic search does not consider the robot’s energy constraints. If the robots are battery-powered, it is physically not possible to continuously explore a space on a single battery charge. Our paper tackles this challenge by integrating ergodic search methods with energy-aware coverage. We trade off battery usage and coverage quality, maintaining uninterrupted exploration of a given space by at least one agent. Our approach is to derive an abstract battery model for future state-of-charge estimation and extend canonical ergodic search to ergodic search under battery constraints. Empirical data from simulations and real-world experiments demonstrate the effectiveness of our energy-aware ergodic search, which ensures continuous and uninterrupted exploration and guarantees spatial coverage.

## I. INTRODUCTION

Robotic exploration is a recurring problem in different scenarios. It typically involves coverage path planning (CPP), which deals with deriving robots’ trajectories that traverse every point in a given space [1–3]. Within CPP, ergodic search is a recent and promising direction [4–17], as it enhances the efficiency of traditional CPP by optimizing the time a robot spends in a given region w.r.t. an information measure. As a result, ergodic search derives trajectories so that the robots spend more time in areas with high information density while quickly passing areas with low information density [13, 18]. The user can specify areas of interest, e.g., where the robots should spend more time exploring in a search and rescue scenario [14], where the robots should collect more data in a precision agriculture scenario [16], etc.

Canonical ergodic search indeed derives continuous exploration [5, 15, 19], but it is physically not possible for robots to continue exploring on a single battery charge. Scenarios involving CPP, however, often require that the space is covered continuously. This work enhances the current ergodic search literature by incorporating more traditional energy-aware CPP approaches [20–25], battery- and energy-aware planning [26–29], and planning of energy trade-offs [30, 31]. It answers the question: *Is it possible to tradeoff battery and coverage quality so that there is at least one agent exploring at all times?*

Prior literature has studied ergodic search in manipulation [8], tactile sensing [15], stochastic dynamics [7, 17], distributed information [5], time optimality [14], and active

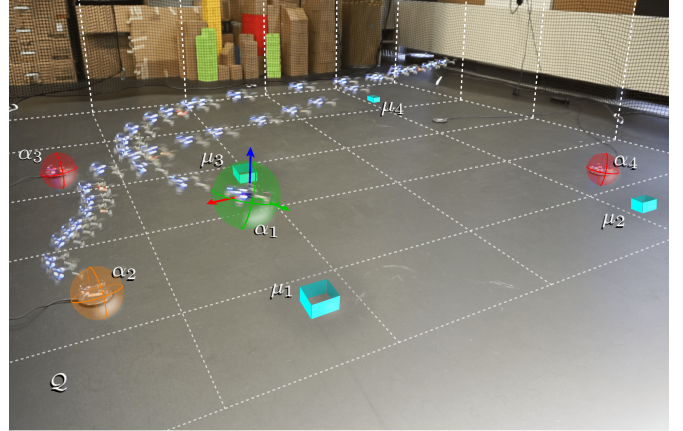


Fig. 1: **Example of energy-aware ergodic search.** A set of agents explores  $\mathcal{Q}$ , focusing on areas with high information density  $\mu_1$ ,  $\mu_2$ ,  $\mu_3$ , and  $\mu_4$ , employing ergodic search. The exploration is continuous and uninterrupted, so that there is always one agent exploring –  $\alpha_1$ , whereas  $\alpha_2$ ,  $\alpha_3$ , and  $\alpha_4$  are recharging. The colors of the spheres indicate the state of charge.

learning [4]. Ergodic search for multi-agent systems [9, 10] has been applied in conjunction with low-information sensors [10–12], swarms control [9], obstacles [11], and decentralized systems [12]. Ergodic search has been proven successful in use cases involving urban environments [13] and information gathering [6]. While prior literature includes ergodic search methods in a variety of settings, energy constraints have not been studied yet. Partly due to these constraints, the uninterrupted exploration that considers a spatial distribution is currently hindered.

Our approach derives an abstract battery model [32] for battery state of charge (SoC) estimation at future time instances. We first adapt canonical ergodic search to multi-agent ergodic search [9, 10]. We then utilize the formulation to propose energy-aware ergodic search, i.e., ergodic search under battery constraints. The exploration is continuous and uninterrupted, employing a finite horizon framework reminiscent of a model predictive controller [29]. Figure 1 shows our setup, which resembles a search and rescue scenario. Four agents explore a space where the high information density is represented by cyan boxes. Some agents are actively exploring, while others are grounded and recharging.

Experimental data from simulations and real-world experiments show the impact of our newly proposed energy-aware ergodic search. We show with empirical evidence that we can effectively explore a space, there is at least one agent exploring, the spatial distribution is satisfied, and the exploration is continuous and uninterrupted (see Section IV). The detailed results from the experimental evaluation and

the code to replicate our approach are made available on the project repository webpage<sup>1</sup>.

The remainder of the paper is structured as follows. Sec. II formulates the problem of multi-agent continuous ergodic search. Sec. III discusses the methods for both the canonical ergodic search and a battery model enhanced ergodic search. Sec. V concludes and proposes future directions.

## II. PROBLEM FORMULATION

This work addresses the problem of exploring a bounded space with multiple agents, proportionally to a spatial distribution and in a such a way that there is at least an agent exploring. In the remainder of the text, we will use the terms *continuously* and *uninterruptedly* to indicate that there is at least one agent that is exploring the space at all times.

Canonical ergodic search [4–8, 18, 19] does not deal with uninterrupted exploration. It derives an agent’s control – or analogously multiple agents control [9–13] – so that its trajectory maximizes an ergodic metric in the spectral domain [33].

**Definition II.1** (Ergodicity). Consider a bounded space  $\mathcal{Q} \subset \mathbb{R}^D$  of dimension  $D \in \mathbb{N}_{>0}$ . A trajectory  $\mathbf{q}(t) \in \mathcal{Q}$  is said *ergodic* with respect to a spatial distribution  $\phi$  if and only if

$$\lim_{t \rightarrow \infty} \frac{1}{t} \int_{\mathcal{T}} \Omega(\kappa(\mathbf{q}(t))) = \int_{\mathcal{Q}} \phi(\mathbf{q}) \Omega(\mathbf{q}) d\mathbf{q}, \quad (1)$$

for all Lebesgue functions  $\Omega$  [18]. The function  $\kappa$  maps the state to exploration space (see Sec. III).

**Definition II.2** (Ergodic metric). Consider a time average distribution that describes where the robot spends more time, i.e.,  $h(\mathbf{q}(t)) = \int_{\mathcal{T}} \Delta(s - \mathbf{q}(t)) dt / t_f$ , where  $s \in \mathcal{Q}$  is a spatial distribution [12] for a finite time  $t_f$ ,  $\Delta$  is a Dirac delta function, and  $t_f \in \mathbb{R}_{>0}$  the final time instant. An *ergodic metric* is defined as the  $L^2$  inner product between the time average distribution  $h$  and the average of the spatial distribution  $\phi$ .

**Problem II.1** (Ergodic search). Consider the bounded space  $\mathcal{Q}$  and a spatial distribution  $\phi$  s.t.  $\int_{\mathcal{Q}} \phi d\mathbf{q} = 1$ ,  $\phi(\mathbf{q}) \geq 0 \forall \mathbf{q} \in \mathcal{Q}$ . *Ergodic search problem* is the problem of deriving a control action  $\mathbf{u}(t) \in \mathcal{U} \subset \mathbb{R}^V$  with  $V \in \mathbb{N}_{>0}$  so that the ergodic metric is minimized (see Definition II.2).

Here the notation  $\mathbb{R}$  and  $\mathbb{N}$  indicates reals and naturals,  $\mathbb{N}_{>0}$  strictly naturals. Bold notation is used for vectors.

We derive an ergodic metric in Equation (3) in Sec. III-A.

We extend the canonical ergodic search problem to energy-aware ergodic search, i.e., uninterrupted exploration with multiple agents under spatial distribution and battery constraints.

**Problem II.2** (Energy-aware ergodic search). Consider a set of  $n$  agents  $\alpha := \{\alpha_1, \alpha_2, \dots, \alpha_n\}$ , a bounded space  $\mathcal{Q}$ , and a spatial distribution  $\phi$  similar to Problem II.1. *Energy-aware ergodic search problem* is the problem of deriving each agent  $\alpha$  control action  $\mathbf{u}(t)$  so that its trajectory  $\mathbf{q}(t)$  is proportional to the spatial distribution  $\phi$  and

the ergodic metric calculated between the agents’ averaged time average distribution in Definition II.2 is satisfied, i.e.,  $\sum_{k \in [n]} \int_{\mathcal{T}} \Delta(s - \mathbf{q}(t)) dt / (n t_f) \leq \gamma$  for a given  $\gamma$ .

We will provide a solution to Problem II.2 (see Sec. III), assuming that there are one or more areas in  $\mathcal{Q}$  – namely, charging stations – where the agents can land and recharge the battery, using, e.g., wireless charging (see Sec. IV).

## III. METHODS

In this section, we discuss the methods utilized in this work for continuous, uninterrupted exploration with multiple agents and proportionally to a spatial distribution

We discuss how to achieve the latter in Sec. III-A and the former in Sec. III-B.

### A. Ergodic search

To derive an agent’s trajectory proportionally to a spatial distribution, canonical ergodic search first requires defining the distribution  $\phi$ .

For this purpose, in both Problem II.1 and II.2, let us consider a Gaussian mixture model (GMM)

$$\phi(\delta, \mathbf{q}) := \sum_{k=1}^m \delta_k \mathcal{N}(\mathbf{q} | \mu_k, \Sigma_k), \quad (2)$$

composed of  $m$  Gaussians. Each has a covariance matrix  $\Sigma_k \in \mathbb{R}^{D \times D}$ , a center  $\mu_k \in \mathcal{Q}$ , and a positive mixing coefficient  $\delta_k \in \delta$  such that the sum of the  $\delta$ s is  $\leq 1$ .

The goal of the ergodic search is to minimize an ergodic metric [18] (see Definition II.2)

$$\mathcal{E}(\delta, \mathbf{q}(t)) := \frac{1}{2} \sum_{k \in \mathcal{K}} \Lambda_k (c_k(\mathbf{q}(t)) - \phi_k(\delta))^2, \quad (3)$$

where  $\phi_k$  are coefficients derived utilizing the Fourier series on the spatial distribution  $\phi$  and  $c_k$  on the trajectory  $\mathbf{q}(t)$ . They are detailed in Eq. (7) and (5) respectively.  $\Lambda_k$  is a weight factor. That is, if

$$\Lambda_k = (1 + \|k\|^2)^{-(D-1)/2}, \quad (4)$$

lower frequencies have more weight [5].  $\mathcal{K} \in \mathbb{N}^D$  is a set of index vectors that covers  $[K] \times \dots \times [K] \in \mathbb{N}^{K^D}$  where  $K$  is a given number of frequencies with the fundamental frequency [33].  $[K]$  indicates positive naturals up to  $K$ .

An agent whose trajectory  $\mathbf{q}(t)$  minimizes Eq. (3) for  $t \rightarrow \infty$  is *optimally ergodic* w.r.t.  $\phi$  [12].

The coefficients  $c_k$  are derived using the Fourier series basis function. If we consider the trigonometric form, they can be expressed

$$c_k(\mathbf{q}(t)) := \int_{\mathcal{T}} \frac{1}{L^D} \prod_{d \in [D]_{>0}} (\cos(k_d \mathbf{q}_d(\tau) \psi) - i \sin(k_d \mathbf{q}_d(\tau) \psi)) d\tau / t, \quad (5)$$

where  $\psi$  is  $2\pi/L$  for a given period  $L \in \mathbb{R}_{>0}$ ,  $i$  is the imaginary unit,  $k_d$  is the  $d$ th item of  $k$ ,  $\mathbf{q}_d$  the  $d$ th item of  $\mathbf{q}$ .

The interval  $\mathcal{T}$  is built so that the integration is between  $\tau = t_0$  and  $t$ , and the notation  $[D]_{>0}$  indicates strictly positive naturals up to  $D$ .

The coefficients  $c_k$  are evaluated per each  $k$  in  $\mathcal{K}$  in Eq. (3).

<sup>1</sup>[github.com/adamseew/enerergo](https://github.com/adamseew/enerergo)

To derive the coefficients  $\phi_k$ , let us consider the GMM model in Eq. (2) on a search space  $\mathcal{Q}$ . The space is further bounded to a symmetric set  $[-L/2, L/2]^D$  since the Gaussians are symmetric about the zero axes. The resulting new model is then

$$\Phi(\delta, \mathbf{q}) := \sum_{d \in [2^D]_{>0}} \sum_{k=1}^m \delta_k \mathcal{N}(\mathbf{q} | A_d \mu_k, A_d \Sigma_k A_d^T) / 2^D, \quad (6)$$

where  $A_d \in \mathbb{R}^{D \times D}$  are linear transformation matrices [33].

Let us call the integrand in Eq. (5)  $c : \mathcal{Q} \rightarrow \mathbb{R}^K$ . It maps the space to the spectral domain. The equivalent of Eq. (5) for the spatial distribution can be then expressed

$$\phi_k(\delta) := \int_{\mathcal{Q}} \Phi(\delta, \mathbf{q}) c(\mathbf{q}) d\mathbf{q}. \quad (7)$$

The space  $\mathcal{Q}$  is built so that the integration is within the points of the bounded symmetric set  $\mathbf{q} \in [-L/2, L/2]^D$ .

The coefficients  $\phi_k$  is evaluated per each  $k$  in  $\mathcal{K}$  in Eq. (3).

Let us first formulate the solution to Problem II.1, utilizing a formulation borrowed from canonical ergodic search. If the agent's dynamics is described by a generic differential equation  $\dot{\mathbf{q}}(t) = f(\mathbf{q}(t), \mathbf{u}(t))$ , an optimal control problem (OCP) that selects an ergodic control action can be formulated as [17]

$$\min_{\mathbf{q}(t), \mathbf{u}(t)} \int_{\mathcal{T}} \mathbf{u}(\tau)^T R \mathbf{u}(\tau) d\tau + \mathcal{E}(\delta, \mathbf{q}(t)), \quad (8a)$$

$$\text{s.t. } \dot{\mathbf{q}} = f(\mathbf{q}(t), \mathbf{u}(t)), \quad (8b)$$

$$\mathbf{q}(t) \in \mathcal{Q}, \mathbf{u}(t) \in \mathcal{U}, \quad (8c)$$

$$\mathbf{q}(t_0), \mathbf{q}(t_f) \text{ are given}, \quad (8d)$$

where the ergodic metric is derived in Eq. (3),  $R \in \mathbb{R}^{V \times V}$  is a control penalizing diagonal positive-definite matrix, and  $t_0, t_f$  are respectively the first and last time instants. The interval  $\mathcal{T}$  is  $[t_0, t_f]$ .

To formulate the solution to Problem II.2, let us first extend the OCP in Eq. (8) to multi-agent systems [10]. Eq. (8a) becomes

$$\min_{\Theta} \frac{1}{n} \left( \sum_{k=1}^n \int_{\mathcal{T}_k} {}^k \mathbf{u}(\tau)^T R_k {}^k \mathbf{u}(\tau) d\tau \right) + \mathcal{E}(\delta, \Theta_{\mathbf{q}}), \quad (9)$$

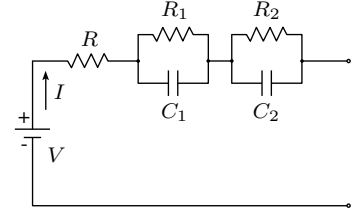
where the ergodic metric and the control penalizing term  $R_k$  are now agent-specific. The term  $\Theta_{\mathbf{q}}$  is  ${}^1 \mathbf{q}(t), {}^2 \mathbf{q}(t), \dots, {}^n \mathbf{q}(t)$ , and  $\Theta$  is  $\Theta_{\mathbf{q}}, {}^1 \mathbf{u}(t), {}^2 \mathbf{u}(t), \dots, {}^n \mathbf{u}(t)$ .  $\mathcal{T}_k$  is  $[{}^k t_0, {}^k t_f]$ , i.e., different agents might have different durations.

The ergodic metric is now evaluated for multiple agents

$$\mathcal{E}(\delta, \Theta_{\mathbf{q}}) := \frac{1}{2} \sum_{k \in \mathcal{K}} \Lambda_k \left( \frac{1}{n} \sum_{j \in [n]} c_k({}^j \mathbf{q}(t)) - \phi_k(\delta) \right)^2. \quad (10)$$

Let us consider a vector  $\mathbf{b} \in \mathbb{R}^3$  – which is detailed later in Sec. III-B – whose trajectory  $\mathbf{b}(t)$  describes the battery metrics' evolution in time. If  $\mathbf{b}_{\text{SoC}}$  is the value of the vector that expresses the battery SoC, the expression in Eq. (9) might select ergodic metrics corresponding to trajectories that are impossible to traverse in the  $\mathbf{b}_{\text{SoC}} \in (0, 1]$  domain.

Fig. 2: **Abstract equivalent circuit model** for state-of-charge estimation [34]. The model consists of a second-order resistor-capacitor circuit with two resistors  $R_1$  and  $R_2$  and two capacitors  $C_1$  and  $C_2$  in two separate circuit elements. An additional resistor  $R$  is also employed.



In order to satisfy the battery SoC domain and always keep at least one agent exploring, an OCP must satisfy an additional constrain

$$\exists k \in [n] \text{ s.t. } {}^k \mathbf{b}_{\text{SoC}}(t_f) \in (0, b_f], \quad (11)$$

where  $b_f \in (0, 1] \subset \mathbb{R}_{>0}$  is a given desired battery SoC at the final time instant.

Finally, let us consider the realistic assumption that the optimization horizon is known and is, e.g., an empirically collected value that corresponds to one of the agents' discharge times (see Sec. IV).

The OCP that provides a solution to Problem II.2 can be formulated as

$$\min_{\Theta} \frac{1}{n} \sum_{k=1}^n \int_{\mathcal{T}_k} {}^k \mathbf{u}(\tau)^T R_k {}^k \mathbf{u}(\tau) d\tau, \quad (12a)$$

$$\text{s.t. } {}^1 \dot{\mathbf{q}}(t) = f_1({}^1 \mathbf{q}(t), {}^1 \mathbf{u}(t)), \dots, {}^n \dot{\mathbf{q}}(t) = f_n({}^n \mathbf{q}(t), {}^n \mathbf{u}(t)), \quad (12b)$$

$${}^1 \mathbf{q}(t), \dots, {}^n \mathbf{q}(t) \in \mathcal{Q}, {}^1 \mathbf{u}(t), \dots, {}^n \mathbf{u}(t) \in \mathcal{U}, \quad (12c)$$

$$\exists k \in [n] \text{ s.t. } {}^k \mathbf{b}_{\text{SoC}}(t_f) \in (0, b_f], \quad (12d)$$

$$\mathcal{E}(\delta, \Theta_{\mathbf{q}}) \leq \gamma, \quad (12e)$$

$$g_1(\delta, {}^1 \mathbf{q}(t), {}^1 \mathbf{u}(t)) \leq 0, \dots, g_n(\delta, {}^n \mathbf{q}(t), {}^n \mathbf{u}(t)) \leq 0, \quad (12f)$$

$${}^1 \mathbf{q}(t_0), {}^1 \mathbf{q}(t_f), \dots, {}^n \mathbf{q}(t_0), {}^n \mathbf{q}(t_f), b_f, \gamma \text{ are given}, \quad (12g)$$

where constraints in Eq. (12f) are optional and express additional requirements, e.g., that there is always at least one agent exploring  $\mathcal{Q}$ , the agents explore the space two-by-two, etc. (see Sec. IV). In Eq. (12), the ergodic metric is integrated into the constraint as proposed in [14].

Furthermore, the evolutions of the agents' states in time are described by generic differential equations  ${}^k \dot{\mathbf{q}}(t) = f_k({}^k \mathbf{q}(t), {}^k \mathbf{u}(t)) \forall k \in [n]$  [12].

## B. Battery modeling

To derive a battery model for continuous exploration – a model that allows us to predict when an agent is exploring and when it conversely should be recharging the battery – let us consider an abstract equivalent circuit model (ECM). These models are commonly employed in battery metrics estimation for robots and other applications, especially if equipped with rechargeable battery cells [29, 35–39].

The ECM model we employ is a second-order resistor-capacitor (RC) circuit model [32], as illustrated in Fig. 2 [34].

Formally, it can be formulated as

$$\dot{\mathbf{b}}(t) = \begin{bmatrix} -1/(R_1 C_1) & 0 & 0 \\ 0 & -1/(R_2 C_2) & 0 \\ 0 & 0 & 0 \end{bmatrix} \mathbf{b}(t) + \begin{bmatrix} 1/C_1 \\ 1/C_2 \\ -\zeta/Q \end{bmatrix} I(t), \quad (13)$$

where  $\zeta \in \mathbb{R}$  is a battery coefficient [29],  $R_1, R_2 \in \mathbb{R}$  and  $C_1, C_2 \in \mathbb{R}$  are the resistors and capacitors relative to the first



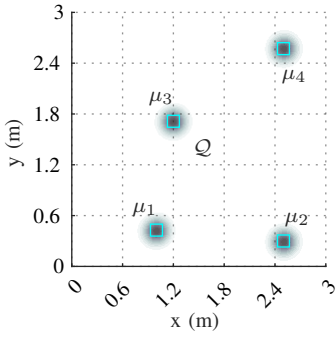


Fig. 3: **Information spatial distribution and search space** in our experimental evaluation. The distribution consists of four Gaussians in a Gaussian mixture model  $\phi$ . The Gaussians are centered in  $\mu_1$ ,  $\mu_2$ ,  $\mu_3$ , and  $\mu_4$ , as depicted by the cyan empty squares. The search space  $\mathcal{Q}$  is a three-by-three area. The resulting ergodic trajectories are expected to be s.t. the robot spends more time close to the Gaussians.

and second RC elements in the ECM measured in ohms and farads respectively.  $Q \in \mathbb{R}$  is the battery nominal capacity measured in amperes per hour.

$I \in \mathbb{R}$  is then the internal current which is load-dependent, e.g., the current required to run the motors, actuators, etc. It is measured in amperes and assumed constant in flight from empirical observations of the aerial vehicles used in the experiments (see Sec. IV).

The state  $\mathbf{b} := [V_1 \ V_2 \ \mathbf{b}_{\text{SoC}}] \in \mathbb{R}^3$  contains three battery metrics.  $V_1, V_2 \in \mathbb{R}$  are the voltages measured in volts across the first and second RC elements, and  $\mathbf{b}_{\text{SoC}} \in (0, 1]$  is the normalized battery SoC that evolves from fully charged – or from a given initial value  $\mathbf{b}_{\text{SoC}}(t_0)$  – to discharged.

The battery voltage at the extremes of the ECM  $V_e \in \mathbb{R}$ , measured in volts, can be then formulated as

$$V_e(t) = V(\mathbf{b}_{\text{SoC}}(t)) - V_1(t) - V_2(t) - I(t)R, \quad (14)$$

where  $R \in \mathbb{R}$  is the single resistor measured in ohms in Fig. 2, and  $V$  the open circuit voltage. It is a function of the battery SoC and can be retrieved from the data sheet [38].

The values of  $R_1, C_1, R_2, C_2, R$  are identified so that the model output and the physical behavior of the agents are matched as closely as possible [32] (see Sec. IV).

The battery model allows us to determine the battery SoC  $\mathbf{b}_{\text{SoC}}$  in Eq. (12d), which is in turn utilized to find the control action  $\mathbf{u}(t)$  so that there is at least one agent exploring  $\mathcal{Q}$  at all times. This means that when the solution of the OCP in Eq. (12) is evaluated, the battery model in Eq. (13) is integrated for the duration of the horizon, whereas

the recharging is approximated linear with the expression  $\mathbf{b}_{\text{SoC}} = \eta \mathbf{b}_{\text{SoC}} + \theta$  for given  $\eta, \theta \in \mathbb{R}$  determined empirically.

#### IV. EXPERIMENTAL RESULTS

In this section, we discuss our experimental setup and results. Our experiments are implemented first in simulation using MATLAB (R), and physical experiments are implemented in Python and conducted using a set of Crazyflie 2.0 micro aerial vehicles (MAVs). The dynamics  $\dot{\mathbf{q}} = f(\mathbf{q}, \mathbf{u})$  is that of a 2D single integrator system, which mimics the MAV control reasonably [14]. The chosen dynamics is not specific to our implementation. The physical experimental setup is illustrated in Fig. 1.

The source code<sup>1</sup> is released under the popular non-commercial open-source license CC BY-NC-SA 4.0. The solution of the OCP in Eq. (12) relies on two external open-source components from the literature: the popular nonlinear programming solver IPOPT [40] and a software framework for nonlinear optimization called CasADi [41].

Each MAV is equipped with a positioning and wireless charging decks. Precise positioning of MAVs is achieved via two HTC SteamVR Base Station 2.0 units. Each MAV is then equipped with a one-cell 250 mAh 3.7 volts LiPo battery.

We evaluate our approach under two different scenarios. In both the scenarios, we use a three-by-three-meter space  $\mathcal{Q}$ . The spatial distribution  $\phi$  contains four Gaussians in the GMM in Eq. (2) in the second scenario, as illustrated in Fig. 3 (the four cyan empty squares). In the first scenario, it contains one Gaussian centered in  $\mu_2$  first, and it contains two Gaussians centered in  $\mu_2$  and  $\mu_3$  later.

##### Competing exploration

In the first scenario, four MAVs  $\alpha_1, \alpha_2, \alpha_3$ , and  $\alpha_4$  are placed on top of four wireless charging stations. The horizon is set to two and a half minutes and is derived empirically along with battery and recharging coefficients. The battery values used in the scenario are those proposed in [32]. The number of frequencies  $K$  is set to nine, as in [33]. The MAVs compete for the same area with high information density, i.e., they utilize the multi-agent ergodic metric introduced in Eq. (10).

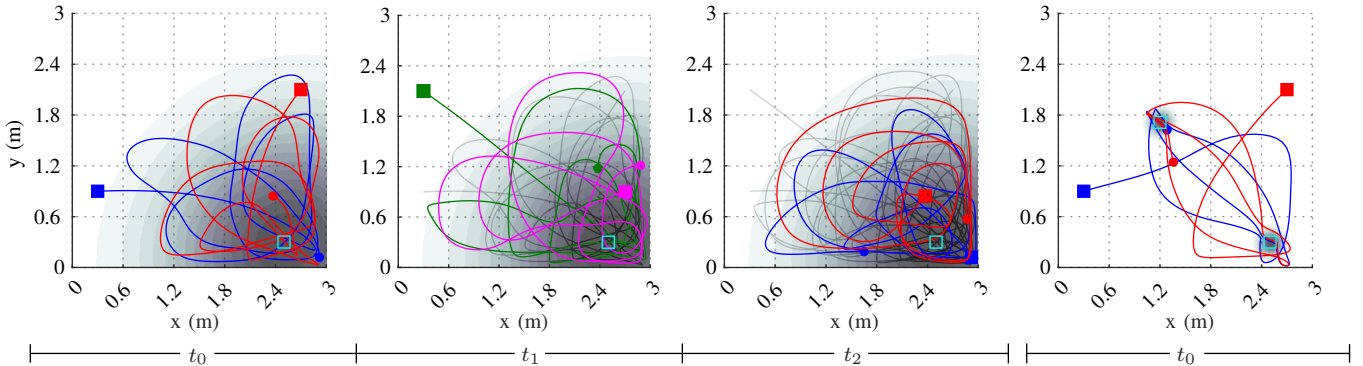


Fig. 4: **Experimental evaluation of competing exploration.** Four agents  $\alpha_1, \alpha_2, \alpha_3$ , and  $\alpha_4$  are placed on top of four wireless charging stations at coordinates (0.3,0.9), (2.7,2.1), (0.3,2.1), and (2.7,0.9). The problem is set so that the agents explore the space two-by-two first, and they compete for one area with high information density – first three sub-figures from left. The same problem is then applied for two areas – last sub-figure. The agents  $\alpha_1$  “blue” and  $\alpha_2$  “red” explore the space in the first horizon  $t_0$  (left of the figure), spending most of the time close to the Gaussian. The agents then return to the charging station to recharge the battery. The other two agents  $\alpha_3$  “dark-green” and  $\alpha_4$  “magenta” proceed for the following horizon. After that, the “blue” and “red” agents resume the previous exploration.

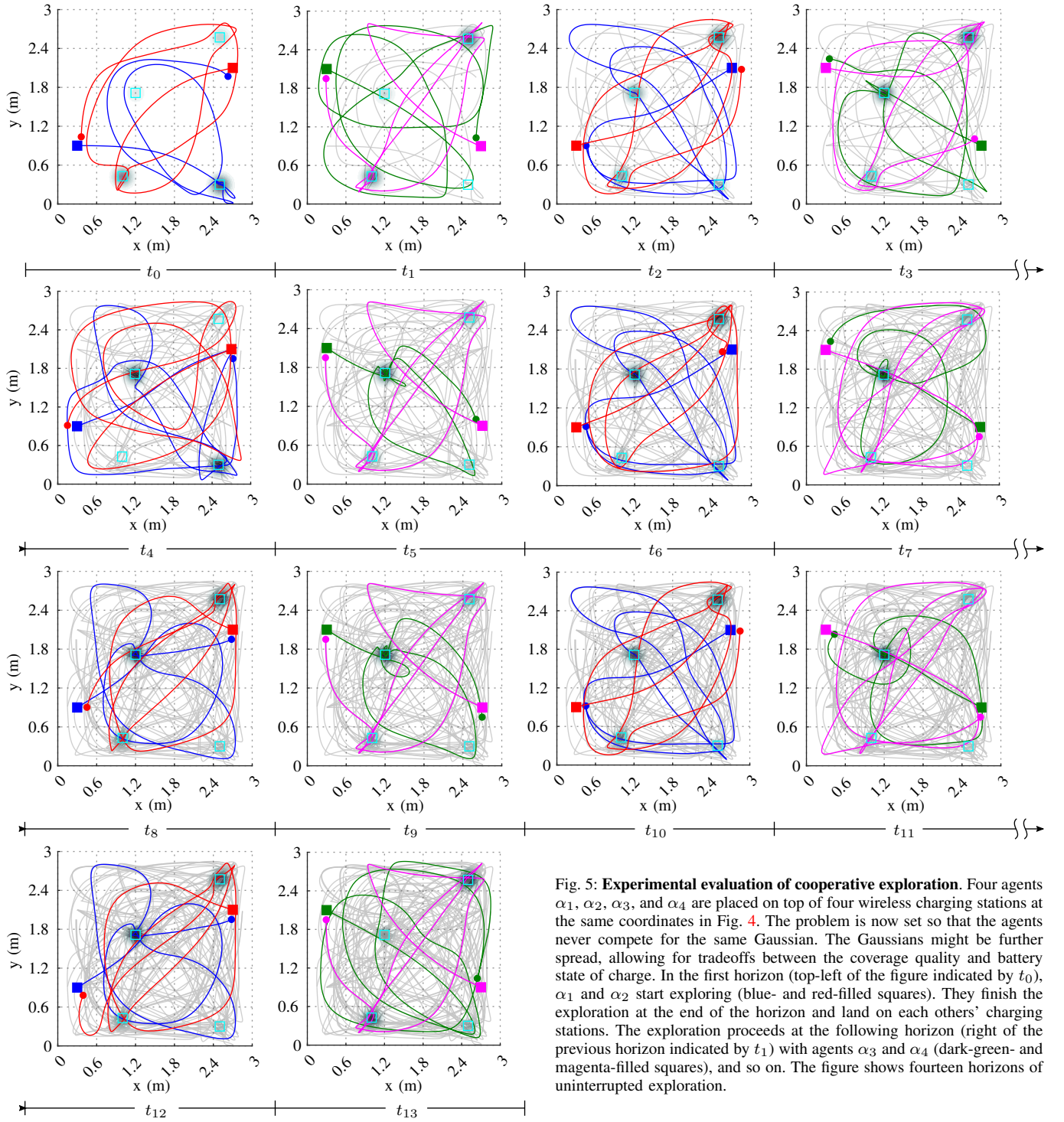


Fig. 5: **Experimental evaluation of cooperative exploration.** Four agents  $\alpha_1$ ,  $\alpha_2$ ,  $\alpha_3$ , and  $\alpha_4$  are placed on top of four wireless charging stations at the same coordinates in Fig. 4. The problem is now set so that the agents never compete for the same Gaussian. The Gaussians might be further spread, allowing for tradeoffs between the coverage quality and battery state of charge. In the first horizon (top-left of the figure indicated by  $t_0$ ),  $\alpha_1$  and  $\alpha_2$  start exploring (blue- and red-filled squares). They finish the exploration at the end of the horizon and land on each others' charging stations. The exploration proceeds at the following horizon (right of the previous horizon indicated by  $t_1$ ) with agents  $\alpha_3$  and  $\alpha_4$  (dark-green- and magenta-filled squares), and so on. The figure shows fourteen horizons of uninterrupted exploration.

The battery constraint is edited so that there are two MAVs first, i.e.,

$$\exists_{=1} k_1, k_2 \in [n] \text{ s.t. } {}^{k_1}\mathbf{b}_{\text{SoC}}, {}^{k_2}\mathbf{b}_{\text{SoC}} \in (0, b_f], \quad (15)$$

where  $\exists_{=1}$  indicates the unique existential quantification.

Initially, two MAVs are selected via the solution to the OCP in Eq. (12),  $\alpha_1$  “blue” and  $\alpha_2$  “red”. They are located at coordinates (0.3,0.9) and (2.7,2.1) respectively, denoted by the blue and red filled squares. The MAVs explore the space for the first horizon, focusing on the area with high

information density (cyan empty square). At the end of the horizon (blue and red filled dots), the MAVs return to the charging stations.

Once the two agents  $\alpha_1$  and  $\alpha_2$  land, they start recharging. The formulation of the OCP in Eq. (12) is such that the other two agents  $\alpha_3$  “dark-green” and  $\alpha_4$  “magenta” are selected. They are located at coordinates (0.3,2.1) and (2.7,0.9).

In the following horizon, the agents  $\alpha_3$  and  $\alpha_4$  are recharging whereas  $\alpha_1$  and  $\alpha_2$  proceed with the exploration from where they left.

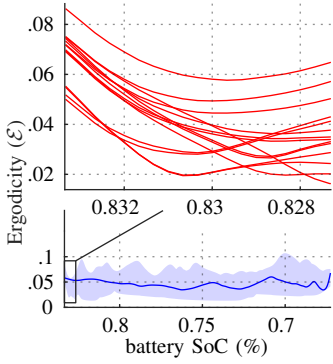


Fig. 6: **Ergodicity as a function of state-of-charge.** The top plot shows the evolution of the ergodicity for all the horizons in Fig. 5. The bottom shows the average ergodicity. Initially, the MAVs are at their charging stations. As they start exploring, they move to the areas with high information density – ergodicity decreases. As they approach the end of the horizon, they start moving to the charging stations – ergodicity increases. The average ergodicity can be observed to be under the value  $\gamma$ .

Last sub-figure in Fig. 4 illustrates the case of the agents competing for two areas with high information density.

### Cooperative exploration

In the second extensive scenario, four MAVs  $\alpha_1$ ,  $\alpha_2$ ,  $\alpha_3$ , and  $\alpha_4$  are placed on top of four wireless charging stations, as in the previous scenario. The optional constraints in Eq. (12f) are built so that each MAV covers two Gaussians at a time that are respectively farthest ( $\mu_3$  and  $\mu_2$  are the centers of Gaussians covered by the “red” and “dark-green” agents,  $\mu_1$  and  $\mu_4$  are the centers of the Gaussians covered by the “blue” and “magenta” agents in Fig. 5). This means that the MAVs will never compete for the same Gaussian, but will cooperate in the exploration.

There is an additional constraint on the final point in Eq (12g), set so that the agents have to be in the proximity of a charging station. The actual constraint is derived in Eq. (17).

The cost function in Eq. (12a) is further enhanced with the mixing coefficient  $\delta$  in Eq. (2), allowing us to find the tradeoffs between the single Gaussians, the different agents, and the battery SoC. Namely, the cost is

$$\min_{\Theta, \delta} \frac{1}{n} \sum_{k=1}^n \int_{\mathcal{T}_k} {}^k \mathbf{u}(\tau)^T R_k {}^k \mathbf{u}(\tau) d\tau - \frac{1}{n} \sum_{k=1}^m \delta_k. \quad (16)$$

A similar approach is undertaken in prior literature [16], where the ergodic objective is dynamic as more information is gathered, rather than the battery status is changed.

The number of frequencies, battery and recharging coefficients, and the horizon are those used in the previous scenario. The ergodicity metric in Eq. (3) is set to be lower or equal to 0.1 via the constraint in Eq. (12e), in line with similar literature [14].

The results are shown in Fig. 5. The figure is to be read from left to right and from top to bottom, with the horizon being indicated under each subfigure (meaning that  $t_0$  is the first horizon,  $t_1$  is the second horizon, etc.). Initially, two MAVs are selected via the solution to the OCP in Eq. (12),  $\alpha_1$  “blue” and  $\alpha_2$  “red”, similarly to the previous scenario. The energy-aware ergodic trajectories  ${}^1 \mathbf{q}(t)$  and  ${}^2 \mathbf{q}(t)$  are selected so that the MAVs land at each other’s charging stations, i.e.,  ${}^1 \mathbf{q}(t_f) = {}^2 \mathbf{q}(t_0)$  and vice-versa. The mixing coefficients for  $\alpha_1$  are such that  $\delta_2 > \delta_3$ , meaning that the agent  $\alpha_1$  explores in more detail the area delimited by the Gaussian centered in  $\mu_2$ . This is indicated by the darker coloring of the different Gaussians, which is proportional to the optimal value of  $\delta$ .

An analogous situation is to be observed with agent  $\alpha_2$ . To guarantee that both agents land in the proximity of each other’s charging stations (the red and blue filled dots at the end of the trajectories for respectively  $\alpha_2$  and  $\alpha_1$ ), the constraint in Eq. (12g) is evaluated within

$$\|{}^{k_2} \mathbf{q}(t_f) - {}^{k_1} \mathbf{q}(t_0)\| \leq \varepsilon, \quad (17)$$

where  $\varepsilon \in \mathbb{R}_{>0}$  and  $k_1, k_2 \in [n]$  are given.

Once the two agents  $\alpha_1$  and  $\alpha_2$  land, they start recharging. The other two agents  $\alpha_3$  “dark-green” and  $\alpha_4$  “magenta” are selected. They proceed on the respective energy-aware ergodic trajectories and land at each other’s charging stations, with the past trajectory being indicated in the background in gray. The figure shows fourteen horizons. The actual exploration in the scenario, however, is continuous.

### Ergodicity against battery state of charge

We report the evolution of the value of the ergodicity metric in Eq. (3) in time as a function of the battery SoC in Fig. 6. The experimental data are from the cooperative exploration.

The top of the figure shows the evolution per each horizon in Fig. 5 in red, whereas the bottom shows the averaged value in blue. We can observe that the exploration starts at an initial value of ergodicity, which mostly depends on the distance from the charging stations to the components of the GMM (i.e., high information density). The ergodicity decreases as the agents move towards the Gaussians in the spatial distribution GMM. It oscillates as the agents move from one Gaussian to another. In the first half of the horizon, the average ergodicity continues to descend as more information is gathered. In the second, the ergodicity increases, peaking at the end, as the discharged agents return to the charging stations for recharging (i.e., low information density).

## V. CONCLUSION AND FUTURE DIRECTIONS

This work answers the question of whether is it possible to explore a space uninterruptedly, with at least one agent at all times. Our methods are to derive an abstract battery model and extend the canonical ergodic search – a method to derive robots’ trajectories that visit areas with high information density – to energy-aware ergodic search. Experimental data indicate the effectiveness of the battery-constrained exploration. Uninterrupted coverage is achieved with a multi-agent system so that there is always at least one agent exploring and the spatial distribution is satisfied – a statement that we prove with empirical evidence.

A limitation of the current methods is that the charging stations are in fixed positions. To enable real-world use cases, we are currently extending the methods to mobile charging stations, which arise in scenarios such as environmental surveying. Furthermore, energy optimality is not addressed by our methods due to the ergodic metric’s non-convexity and high non-linearity. Future work will explore the possibilities of guaranteeing energy optimality under battery constraints.



## REFERENCES

- [1] H. Choset, "Coverage for robotics—A survey of recent results," *Annals of Mathematics and Artificial Intelligence*, vol. 31, pp. 113–126, 2001. **1**
- [2] E. Galceran and M. Carreras, "A survey on coverage path planning for robotics," *Robotics and Autonomous Systems*, vol. 61, no. 12, pp. 1258–1276, 2013. **1**
- [3] T. a. M. Cabreira, L. B. Brisolará, and P. R. Ferreira Jr., "Survey on coverage path planning with unmanned aerial vehicles," *Drones*, vol. 3, no. 1, 2019. **1**
- [4] I. Abraham, A. Prabhakar, and T. D. Murphey, "An ergodic measure for active learning from equilibrium," *IEEE Transactions on Automation Science and Engineering*, vol. 18, no. 3, pp. 917–931, 2021. **1, 2**
- [5] L. M. Miller, Y. Silverman, M. A. MacIver, and T. D. Murphey, "Ergodic exploration of distributed information," *IEEE Transactions on Robotics*, vol. 32, no. 1, pp. 36–52, 2016. **1, 2**
- [6] L. Dressel and M. J. Kochenderfer, "On the optimality of ergodic trajectories for information gathering tasks," in *IEEE American Control Conference*, 2018, pp. 1855–1861. **1, 2**
- [7] G. De La Torre, K. Flaßkamp, A. Prabhakar, and T. D. Murphey, "Ergodic exploration with stochastic sensor dynamics," in *IEEE American Control Conference*, 2016, pp. 2971–2976. **1, 2**
- [8] S. Shetty, J. Silvério, and S. Calinon, "Ergodic exploration using tensor train: Applications in insertion tasks," *IEEE Transactions on Robotics*, vol. 38, no. 2, pp. 906–921, 2022. **1, 2**
- [9] A. Prabhakar, I. Abraham, A. Taylor, M. Schlafly, K. Popovic, G. Diniz, B. Teich, B. Simidchieva, S. Clark, and T. Murphey, "Ergodic specifications for flexible swarm control: From user commands to persistent adaptation," in *Robotics: Science and Systems*, 2020, p. 9. **1, 2**
- [10] H. Coffin, I. Abraham, G. Sartoretti, T. Dillstrom, and H. Choset, "Multi-agent dynamic ergodic search with low-information sensors," in *IEEE International Conference on Robotics and Automation*, 2022, pp. 11480–11486. **1, 2, 3**
- [11] C. Lerch, D. Dong, and I. Abraham, "Safety-critical ergodic exploration in cluttered environments via control barrier functions," in *IEEE International Conference on Robotics and Automation*, 2023, pp. 10205–10211. **1, 2**
- [12] I. Abraham and T. D. Murphey, "Decentralized ergodic control: Distribution-driven sensing and exploration for multiagent systems," *IEEE Robotics and Automation Letters*, vol. 3, no. 4, pp. 2987–2994, 2018. **1, 2, 3**
- [13] S. Patel, S. Hariharan, P. Dhulipala, M. C. Lin, D. Manocha, H. Xu, and M. Otte, "Multi-agent ergodic coverage in urban environments," in *IEEE International Conference on Robotics and Automation*, 2021, pp. 8764–8771. **1, 2**
- [14] D. Dong, H. Berger, and I. Abraham, "Time optimal ergodic search," in *Robotics: Science and Systems*, 2023, p. 13. **1, 3, 4, 6**
- [15] I. Abraham, A. Prabhakar, M. J. Z. Hartmann, and T. D. Murphey, "Ergodic exploration using binary sensing for nonparametric shape estimation," *IEEE Robotics and Automation Letters*, vol. 2, no. 2, pp. 827–834, 2017. **1**
- [16] A. Rao, A. Breitfeld, A. Candela, B. Jensen, D. Wettergreen, and H. Choset, "Multi-objective ergodic search for dynamic information maps," in *IEEE International Conference on Robotics and Automation*, 2023, pp. 10197–10204. **1, 6**
- [17] E. Ayvali, H. Salman, and H. Choset, "Ergodic coverage in constrained environments using stochastic trajectory optimization," in *IEEE/RSJ International Conference on Intelligent Robots and Systems*, 2017, pp. 5204–5210. **1, 3**
- [18] G. Mathew and I. Mezić, "Metrics for ergodicity and design of ergodic dynamics for multi-agent systems," *Physica D: Nonlinear Phenomena*, vol. 240, no. 4, pp. 432–442, 2011. **1, 2**
- [19] L. M. Miller and T. D. Murphey, "Trajectory optimization for continuous ergodic exploration," in *IEEE American Control Conference*, 2013, pp. 4196–4201. **1, 2**
- [20] C. Di Franco and G. Buttazzo, "Energy-aware coverage path planning of UAVs," in *IEEE International Conference on Autonomous Robot Systems and Competitions*, 2015, pp. 111–117. **1**
- [21] —, "Coverage path planning for UAVs photogrammetry with energy and resolution constraints," *Journal of Intelligent & Robotic Systems*, vol. 83, no. 3, pp. 445–462, 2016. **1**
- [22] I. Shnaps and E. Rimon, "Online coverage of planar environments by a battery powered autonomous mobile robot," *IEEE Transactions on Automation Science and Engineering*, vol. 13, no. 2, pp. 425–436, 2016. **1**
- [23] T. a. M. Cabreira, C. D. Franco, P. R. Ferreira, and G. C. Buttazzo, "Energy-aware spiral coverage path planning for UAV photogrammetric applications," *IEEE Robotics and Automation Letters*, vol. 3, no. 4, pp. 3662–3668, 2018. **1**
- [24] M. Wei and V. Isler, "Coverage path planning under the energy constraint," in *IEEE International Conference on Robotics and Automation*, 2018, pp. 368–373. **1**
- [25] K. R. Jensen-Nau, T. Hermans, and K. K. Leang, "Near-optimal area-coverage path planning of energy-constrained aerial robots with application in autonomous environmental monitoring," *IEEE Transactions on Automation Science and Engineering*, vol. 18, no. 3, pp. 1453–1468, 2021. **1**
- [26] Y. Mei, Y.-H. Lu, Y. C. Hu, and C. G. Lee, "Energy-efficient motion planning for mobile robots," in *IEEE International Conference on Robotics and Automation*, vol. 5, 2004, pp. 4344–4349. **1**
- [27] —, "A case study of mobile robot's energy consumption and conservation techniques," in *IEEE International Conference on Advanced Robotics*, 2005, pp. 492–497. **1**
- [28] C. H. Kim and B. K. Kim, "Energy-saving 3-step velocity control algorithm for battery-powered wheeled mobile robots," in *IEEE International Conference on Robotics and Automation*, 2005, pp. 2375–2380. **1**
- [29] A. Seewald, H. García de Marina, H. S. Midtiby, and U. P. Schultz, "Energy-aware planning-scheduling for autonomous aerial robots," in *IEEE/RSJ International Conference on Intelligent Robots and Systems*, 2022, pp. 2946–2953. **1, 3**
- [30] P. Ondrúška, C. Gurău, L. Marchegiani, C. H. Tong, and I. Posner, "Scheduled perception for energy-efficient path following," in *IEEE International Conference on Robotics and Automation*, 2015, pp. 4799–4806. **1**
- [31] S. Sudhakar, S. Karaman, and V. Sze, "Balancing actuation and computing energy in motion planning," in *IEEE International Conference on Robotics and Automation*, 2020, pp. 4259–4265. **1**
- [32] S. Zhao, S. R. Duncan, and D. A. Howey, "Observability analysis and state estimation of lithium-ion batteries in the presence of sensor biases," *IEEE Transactions on Control Systems Technology*, vol. 25, no. 1, pp. 326–333, 2017. **1, 3, 4**
- [33] S. Calinon, *Mixture models for the analysis, edition, and synthesis of continuous time series*. Springer, 2020, pp. 39–57. **2, 3, 4**
- [34] A. Seewald, "Energy-aware coverage planning and scheduling for autonomous aerial robots," Ph.D. dissertation, Syddansk Universitet. Det Tekniske Fakultet, 2021, [doi.org/10.21996/7ka6-r457](https://doi.org/10.21996/7ka6-r457). **3**
- [35] C. Zhang, W. Allafi, Q. Dinh, P. Ascencio, and J. Marco, "Online estimation of battery equivalent circuit model parameters and state of charge using decoupled least squares technique," *Energy*, vol. 142, pp. 678–688, 2018. **3**
- [36] X. Hu, S. Li, and H. Peng, "A comparative study of equivalent circuit models for li-ion batteries," *Journal of Power Sources*, vol. 198, pp. 359–367, 2012. **3**
- [37] A. Hasan, M. Skriver, and T. A. Johansen, "eXogenous Kalman filter for state-of-charge estimation in lithium-ion batteries," in *IEEE Conference on Control Technology and Applications*, 2018, pp. 1403–1408. **3**
- [38] H. Hinz, "Comparison of lithium-ion battery models for simulating storage systems in distributed power generation," *Inventions*, vol. 4, 2019. **3, 4**
- [39] S. Mousavi G. and M. Nikdel, "Various battery models for various simulation studies and applications," *Renewable and Sustainable Energy Reviews*, vol. 32, pp. 477–485, 2014. **3**
- [40] A. Wächter and L. T. Biegler, "On the implementation of an interior-point filter line-search algorithm for large-scale nonlinear programming," *Mathematical Programming*, vol. 106, no. 1, pp. 25–57, 2006. **4**
- [41] J. Andersson, J. Åkesson, and M. Diehl, "CasADi: A symbolic package for automatic differentiation and optimal control," in *Recent Advances in Algorithmic Differentiation*. Springer, 2012, pp. 297–307. **4**